Model Predictive-Based Maximum Power Point Tracking for Grid-Tied Photovoltaic Applications Using a *Z*-Source Inverter

Sally Sajadian, *Member, IEEE*, and Reza Ahmadi, *Member, IEEE*

***Abstract*—This paper presents a model predictive-based maximum power point tracking (MPPT) method for a photovoltaic energy harvesting system based on a single-stage grid-tied *Z*-source inverter. First, it provides a brief review of *Z*-source inverters, MPPT methods and model predictive control. Next, it introduces the proposed model predictive-based MPPT method. Finally, it provides experimental results to verify the theoretical outcomes.**

***Index Terms*—Impedance-source inverter, model predictive control (MPC), maximum power point tracking, photovoltaic (PV) systems.**

I. Introduction

PHOTOVOLTAIC (PV) systems are one of the most promising electric power generation systems due to their low environmental impact and high availability of solar irradiation in most geographical locations [1], [2]. The energy generated by the PV systems is highly dependent on the environmental and ambient conditions such as the solar irradiance level and the module temperature. In order to ensure extraction of the maximum available energy in any ambient condition, maximum power point tracking (MPPT) for PV systems is essential [3]. The PV system efficiency can be degraded easily if the PV module is not forced to operate at its maximum power point (MPP) at all times regardless of the environmental conditions.

Conventional grid-tied PV systems typically use a two-stage power conversion topology: an upstream dc/dc power conversion stage from the PV module to a dc-link energy buffer (such as a capacitor), and a downstream dc/ac power conversion stage from the energy buffer to the grid. Several control techniques and analysis have been developed in the literature for each of these conversion stages [4]–[8]. The general schematic of a conventional two-stage grid-tied PV system is illustrated in Fig. 1. The use of a two-stage topology is necessitated due to the inherent limitation of the dc/ac inverters for stepping up/down the voltage freely. Commonly, the conventional inverters classified as voltage-source inverters (VSI) can only step-down the voltage while the current-source inverters (CSI) can only step-up the voltage [9], [10].

Manuscript received October 21, 2015; revised January 08, 2016; accepted February 17, 2016. Date of publication March 03, 2016; date of current version June 24, 2016. Recommended for publication by Associate Editor Y. Liu.

The authors are with the Department of Electrical Engineering and Computer Science, University of Kansas, Lawrence, KS 66045 USA (e-mail: sally.sajadian@gmail.com; ahmadi@ku.edu).

Color versions of one or more of the figures in this paper are available online at http://ieeexplore.ieee.org.

Digital Object Identifier 10.1109/TPEL.2016.2537814

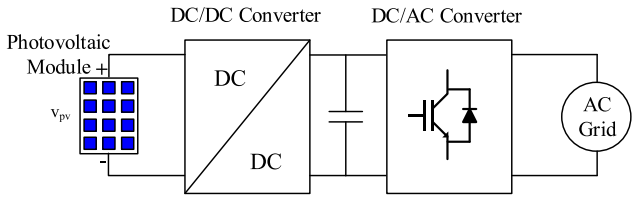

Fig. 1. Two-stage grid-tied PV system configuration.

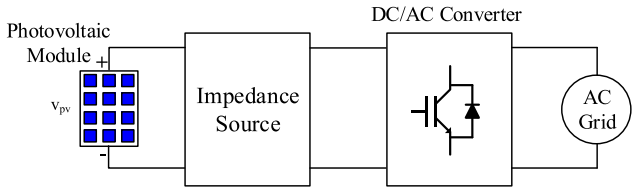

Fig. 2. Single-stage impedance-source grid-tied PV system configuration.

The MPP voltage of a PV module can be higher/lower than the grid voltage based on the environmental conditions, necessitating a power conversion system that can step up/down the voltage freely to track the MPP accurately. Recently, a new converter topology, denoted as the impedance-source converter, is developed by the researchers that undermines the limitations with the conventional VSIs and CSIs [11]–[13]. In particular, a class of dc/ac inverters designed based on the concept of impedance-source conversion, denoted as *Z*-source inverter (ZSI), can step up/down the voltage freely, and thus is very well suited for designing single-stage PV harvesting systems. Fig. 2 demonstrates a single-stage PV harvesting system built around a ZSI.

This paper presents a new MPPT scheme for a ZSI-based PV energy harvesting system based on the concept of model predictive control (MPC). The MPC technique features simplicity and flexibility, and can be programmed to compensate for the inherent nonlinearities associated with power electronic converters. Comparing to classical control schemes, MPC delivers a fast dynamic response with a high stability margin, making it well suited for MPPT of PV systems operating under dynamic environmental conditions. A few research works have been recently published focusing on the MPPT for grid-tied PV system by MPC [14]–[17]. The work presented by Shadmand *et al.* [14], [17] uses a conventional perturb and observe (P&O) algorithm for identification of MPP. However, in the approach presented in this paper, the MPC method is used directly to predict the power generated by the PV panel, subsequent to possible changes to

the PV voltage. Accordingly, in this paper, the decisions on the trajectory of the PV voltage are directly made by a MPC algorithm. This provides advantages to the MPPT process over the conventional methods.

Unlike the previous works, the proposed method uses a fixed switching frequency and an adaptively predicted voltage step that can change according to the proximity to the MPP. This improves the tracking response causes by variations in solar irradiance level and minimizes the oscillation around the MPP. Thus, the proposed MPPT technique features high control effectiveness, fast dynamic response, and small oscillations around MPP without requiring expensive sensing devices to measure the solar irradiance level directly. Due to nature of MPC which predicts the system behavior in a specified time horizon, the most significant advantage of the proposed technique is high accuracy tracking of gradually changing solar irradiance levels, a property absent in most well-known MPPT techniques such as P&O. Moreover, due to small oscillations around MPP, the proposed technique makes it possible to use a ZSI with small inductors/capacitors for the PV harvesting system. This is especially important because according to [18], one of the challenges of employing impedance-source inverters such as ZSIs is the large size of the passive elements in the impedance network. Consequently, by using the proposed method, the foot print of a ZSI converter can be reduced significantly. Although the proposed method can be used in conjunction with other converters, its benefits will signify when used with a ZSI.

This paper is structured as follows: Section II provides a review of the impedance-source converters, the MPPT methods, and the MPC techniques. Section III presents the proposed model predictive-based MPPT technique and the new PV harvesting system built around the ZSI. Section IV provides experimental results to validate the operation of the proposed system. Section V concludes this paper.

II. Groundworks

A. Impedance-Source Converters

The impedance networks can be utilized in a wide range of power conversion applications to provide a flexible means of conversion between different types of sources and loads [19]–[22]. A simple impedance-source converter, denoted as a ZSI in the literature [9], [12], [13], [23], [24] is utilized as the PV harvesting interface in this paper. A distinctive characteristic of a ZSI is its capability to leverage shoot-through switching states for boosting the output voltage [11]. In shoot-through states, both switches in one leg of the inverter are turned ON simultaneously. Due to inclusion of the shoot-through states, controlling ZSIs requires innovative modulation strategies. Several novel modulation strategies based on pulse width modulation (PWM) method have been proposed for ZSIs in the literature lately [9], [25], [26]. Three notable modulation strategies for ZSIs are simple-boost [11], maximum-boost [23], and constant-boost [24] techniques. In this paper, the simple boost strategy is chosen for generating the switching signals for the ZSI of Fig. 3.

The simple boost modulation strategy operates similar to a traditional carrier-based PWM [27] and its voltage gain is given by [11]

$$G = MB = \frac{V_{\rm ac}}{V_0/2} = \frac{M}{2M-1} \tag{1}$$

where M is the modulation index, B is the boosting factor of the impedance-network, $V_{\rm ac}$ is the amplitude of the output voltage of the inverter (equivalent to grid peak phase voltage when grid-tied), and V_0 is the dc-link voltage. The boosting factor B is given by [26]

$$B = \frac{1}{1-2D} \tag{2}$$

where D is the shoot-through duty ratio.

B. MPPT Techniques

Fast convergence, small power ripple at MPP, and accurate and robust tracking of MPP are the key desired properties of a MPPT technique. Several algorithms, architectures, and mechanisms for tracking the MPP of a PV module have been proposed in the literature in the past two decades. Some of the very well-known MPPT methods include: hill-climbing algorithm [28], power-matching scheme [29], curve-fitting technique [30], [31], P&O algorithm [32], [33], incremental conductance algorithm [34], and fractional open-circuit voltage ($V_{\rm oc}$) control [35]. In this work, the idea behind the P&O algorithm is used as grounds to develop the new model predictive-based MPPT technique that features better energy harvesting efficacy which can more effectively hedge against dynamic environmental conditions.

C. MPC for Power Electronic Converters

Power electronic converters are nonlinear systems with finite number of switching devices that need to be controlled according to stringent operational goals and constraints. Controlling power electronic converters with the aforementioned characteristics demands for elaborate control schemes. As such, the MPC technique has been emerging lately as a promising new control strategy for control of power electronic systems [36], [37]. Comparing to classical control schemes, MPC techniques deliver a fast dynamic response with a high stability margin, making them well suited for MPPT of PV systems operating under dynamic environmental conditions.

The MPC techniques use the discrete-time model of the system to evaluate the predicted value of system states and use the predictions to determine an optimal switching schedule for the future steps that will minimize a predefined cost function. Designing an MPC scheme involves the following steps [36]: 1) identifying all possible switching configurations of the converter and deriving the discrete-time model of the converter for each configuration. The derived models allow to predict future values of the system such as output voltage or current; 2) defining a cost function that upon minimization leads to the desired behavior of the system; 3) predicting the behavior of the system states for all possible switching configurations; and 4) evaluating the cost function for each possible switching configuration and selecting the switching configuration for the next step that minimizes the cost function.

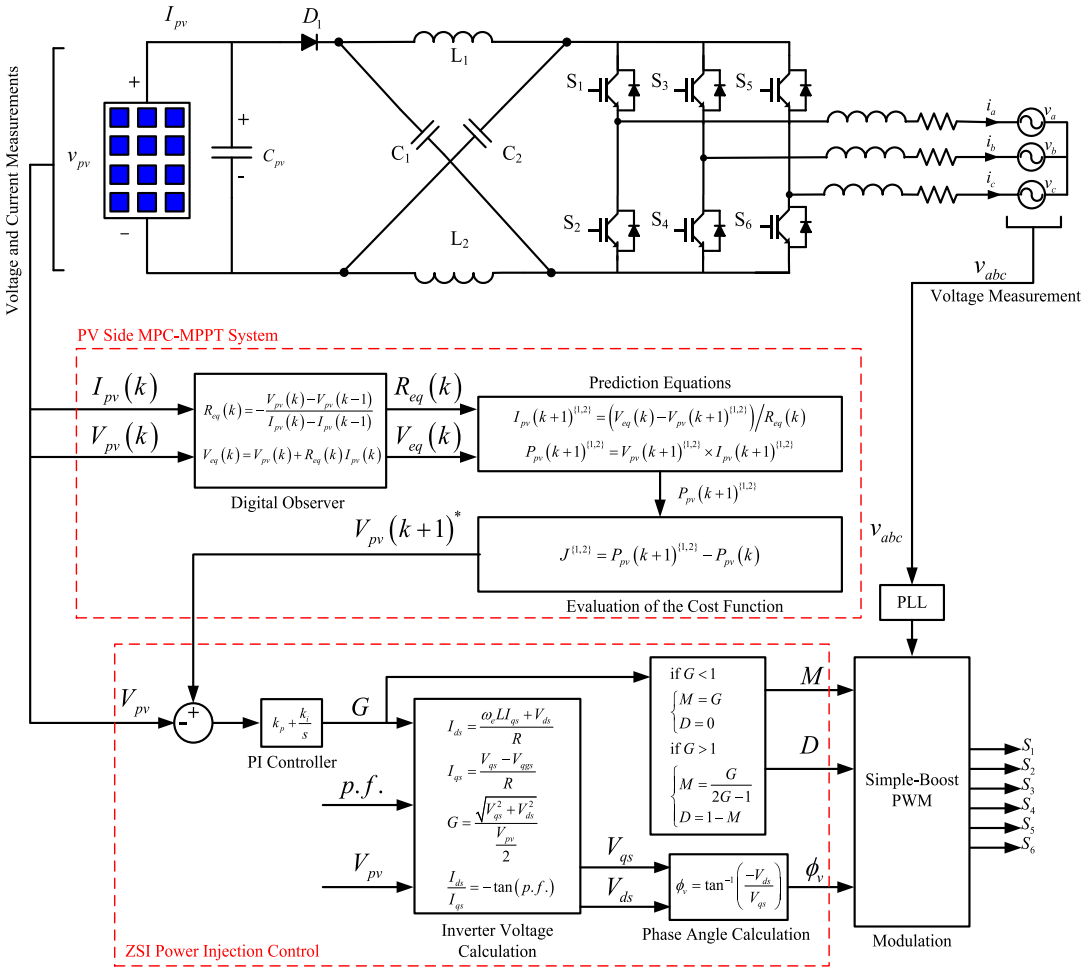

Fig. 3. Grid-tied ZSI and the block diagram of the proposed control system.

III. Proposed Model Predictive-Based MPPT

The grid-tied ZSI and the block diagram of the proposed MPPT system for this converter are illustrated in Fig. 3. The overall control system is comprised of two parts: the PV-side model predictive-based MPPT and the grid-side ZSI power injection control.

A. PV-Side Model Predictive-Based MPPT

The proposed model predictive-based MPPT algorithm tracks the MPP of the PV module by shifting the PV voltage to the voltage at MPP through the following steps.

Step 1: At any given sample time k (referred to as the "current sample time" hereinafter) during the operation, the ZSI can be commanded to either increase or decrease the PV voltage $V_{\rm pv}(k)$. As a result, there are two possible values for the future PV voltage $V_{\rm pv}(k+1)$ at sample time $k+1$ (referred to as "next sample time" hereinafter). In the first step, the algorithm calculates the two possible future PV voltage values

$$\begin{aligned} V_{\rm pv}(k+1)^1 &= V_{\rm pv}(k)+\Delta V \\ V_{\rm pv}(k+1)^2 &= V_{\rm pv}(k)-\Delta V \end{aligned} \tag{3}$$

where ΔV is a voltage step which is an adaptively predicted value that can change according to the proximity to the MPP. In this work, the following update law for ΔV is proposed:

$$\Delta V = \left|\tilde{V}_{\rm pv}^{\rm ave}(k+1) - V_{\rm pv}(k)\right| \tag{4}$$

where $\tilde{V}_{\rm pv}^{\rm ave}(k+1)$ is the predicted average PV voltage for the next sample time $(k+1)$. The procedure of finding $\tilde{V}_{\rm pv}^{\rm ave}(k+1)$ is explained at the end of this section.

Step 2: In this step, the algorithm calculates (predicts) the power that would be drawn from the PV module if the PV voltage where to shift to either of the two possible values of $V_{\rm pv}(k+1)^1$ or $V_{\rm pv}(k+1)^2$, in the next sample time. To predict the generated power, the algorithm requires the knowledge of the local P–V characteristic of the module around the operating point of $V_{\rm pv}(k)$. In this work, a digital observer is designed to generate the required knowledge for the predictions. The digital observer models the PV module with the Thevenin circuit of Fig. 4. The elements of this circuit, the equivalent voltage $V_{\rm eq}$, and equivalent resistance $R_{\rm eq}$ of the module are functions of the P–V characteristic of the PV module and subject to local estimation by the digital observer. The employed estimator

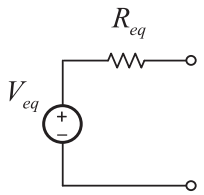

Fig. 4. Equivalent circuit model of the PV module.

equations are

$$\begin{aligned} R_{\mathrm{eq}}(k) &= -\frac{V_{\mathrm{pv}}(k)-V_{\mathrm{pv}}(k-1)}{I_{\mathrm{pv}}(k)-I_{\mathrm{pv}}(k-1)} \\ V_{\mathrm{eq}}(k) &= V_{\mathrm{pv}}(k)+R_{\mathrm{eq}}(k)\,I_{\mathrm{pv}}(k) \end{aligned} \tag{5}$$

where $V_{\mathrm{pv}}(k-1)$ and $I_{\mathrm{pv}}(k-1)$ are the values of the PV module voltage and current from the previous sampling time. Estimating the equivalent resistance and voltage of the PV module, the two possible values for the generated power in the next sampling time can be easily predicted from

$$P_{\mathrm{pv}}(k+1)^1 = V_{\mathrm{pv}}(k+1)^1 \times I_{\mathrm{pv}}(k+1)^1 \tag{6}$$

where

$$I_{\mathrm{pv}}(k+1)^1 = \frac{V_{\mathrm{eq}}(k)-V_{\mathrm{pv}}(k+1)^1}{R_{\mathrm{eq}}(k)} \tag{7}$$

and

$$P_{\mathrm{pv}}(k+1)^2 = V_{\mathrm{pv}}(k+1)^2 \times I_{\mathrm{pv}}(k+1)^2 \tag{8}$$

where

$$I_{\mathrm{pv}}(k+1)^2 = \frac{V_{\mathrm{eq}}(k)-V_{\mathrm{pv}}(k+1)^2}{R_{\mathrm{eq}}(k)}. \tag{9}$$

Step 3: In this step, the predicted power for the two cases will be used to evaluate the following cost function:

$$J^{\{1,2\}} = P_{\mathrm{pv}}(k+1)^{\{1,2\}} - P_{\mathrm{pv}}(k). \tag{10}$$

To increase the generated power in each step, the predicted power, $P_{\mathrm{pv}}(k+1)^1$ or $P_{\mathrm{pv}}(k+1)^2$, that will result in a larger value of J from (10), will be selected as the desirable trajectory for the next step. For instance, if $J^1 > J^2$, then the algorithm chooses to generate $P_{\mathrm{pv}}(k+1)^1$ in the next sampling time, which correspondingly means the PV voltage will need to be shifted to $V_{\mathrm{pv}}(k+1)^1$ by proper adjustment of the inverter gain. The desirable value of the PV voltage for the next step is denoted as $V_{\mathrm{pv}}(k+1)^*$ hereinafter. In order to regulate the PV voltage to $V_{\mathrm{pv}}(k+1)^*$, the inverter gain needs to be adjusted. The ZSI power injection control system described in the next section is responsible for accomplishing this task.

Procedure of finding $\tilde{V}_{\mathrm{pv}}^{\mathrm{ave}}(k+1)$. In order to find the predicted average PV voltage for the next sample time, the discretized average value model of the ZSI needs to be developed. The discretized equations for the ZSI in a shoot through and a non-shoot-through state can be used to develop the average value model. The discretized equations for a nonshoot through state are found in the literature as [38], [39]

$$\begin{cases} I_{L1}(k+1) = I_{L1}(k) + \dfrac{T_S}{L_1}(V_{\mathrm{pv}} - V_{C1}(k) - R_{L1}I_{L1}(k)) \\ V_{C1}(k+1) = V_{C1}(k) + \dfrac{T_S}{C_1}(I_{L1}(k+1) - I_{\mathrm{in}v}(k+1)) \end{cases} \tag{11}$$

where T_S is the sampling time and

$$I_{\mathrm{in}v}(k+1) = S_1 \times I_a(k) + S_2 \times I_b(k) + S_3 \times I_c(k). \tag{12}$$

The discretized equations for the shoot-through state are found similarly from [38], [39]

$$\begin{cases} I_{L1}(k+1) = I_{L1}(k) + \dfrac{T_S}{L_1}(V_{C1}(k) - R_{L1}I_{L1}(k)) \\ V_{C1}(k+1) = V_{C1}(k) - \dfrac{T_S}{C_1}I_{L1}(k+1). \end{cases} \tag{13}$$

$V_{C1}(k+1)$ is assumed to be approximately equal to $V_{C1}(k)$ since the change is minor for sufficiently small sampling time T_S [38], [39]. The average current going through C_{pv} and C_1 should be zero; thus, the I_{PV} is the same as the ZSI inductor current I_{L_1}. Therefore, the predicted average PV current can be formulated using (11) and (13) as

$$\begin{aligned} \tilde{I}_{\mathrm{pv}}^{\mathrm{ave}}(k+1) = {} & \left[I_{L1}(k) + \frac{T_S}{L_1}(V_{\mathrm{pv}} - V_{C1}(k) - R_{L1}I_{L1}(k))\right] \\ & \times (1-D(k)) \\ & + \left[I_{L1}(k) + \frac{T_S}{L_1}(V_{C1}(k) - R_{L1}I_{L1}(k))\right] \\ & \times D(k). \end{aligned} \tag{14}$$

Considering that the relationship between the PV voltage and V_{C1} can be described as [22]

$$V_{\mathrm{pv}} = \frac{2}{B+1}V_{C1}. \tag{15}$$

The average PV voltage can be predicted using (11), (13), and (15) as follows:

$$\begin{aligned} & \tilde{V}_{\mathrm{pv}}^{\mathrm{ave}}(k+1) = \\ & \frac{2}{B+1}\left\{\left[V_{C1}(k) + \frac{T_S}{C_1}(I_{L1}(k+1) - I_{\mathrm{in}v}(k+1))\right]\right. \\ & \times (1-D(k)) + \left.\left[V_{C1}(k) - \frac{T_S}{C_1}I_{L1}(k+1)\right] \times D(k)\right\} \end{aligned} \tag{16}$$

where *B* is the boosting factor.

B. ZSI Power Injection Control

This part of the control system has three goals: regulating the PV voltage to $V_{\mathrm{pv}}(k+1)^*$ provided by the PV-side MPPT system by properly adjusting the inverter gain, controlling the ratio of active/reactive power injected to the grid (power factor (p.f.) control) according to the specific application requirements, and minimizing the voltage stress on the switches. The proposed control system accomplishes the three mentioned goals by generating *M*, *D*, and the phase angle of the inverter voltages ϕ_v.

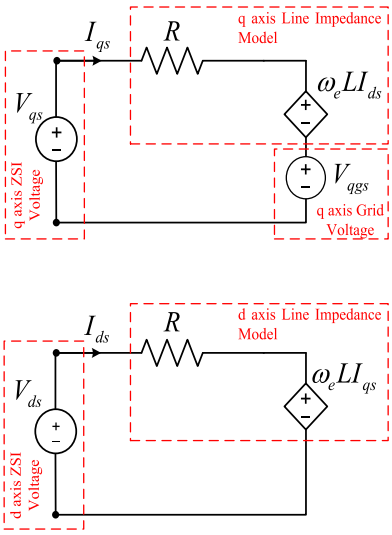

Fig. 5. *q–d* model of the grid-tied ZSI system.

The generated values will be used by the simple-boost modulator to produce proper switching signals for controlling the inverter.

As pictured in Fig. 3, the proposed system uses a proportional-integral controller to regulate the PV voltage to $V_{\rm pv}\ (k+1)^*$ by adjusting the inverter gain. Therefore, the output of the PI controller in Fig. 3 is the inverter gain. The inverter gain generated by the PI controller can be used along with the desired p.f. of the operation to calculate the phase angle of the inverter voltages ϕ_v. To calculate ϕ_v, the inverter system needs to be analyzed in a rotational *q–d* reference frame. The equivalent circuits of the grid-tied ZSI system in the steady-state condition in a *q–d* reference frame synchronized with the grid voltage is shown in Fig. 5 [40]. According to this figure, the *q* and *d*-axis inverter currents,I_{qs} and I_{ds}, can be formulated as

$$I_{ds} = \frac{\omega_e L I_{qs} + V_{ds}}{R}$$
$$I_{qs} = \frac{V_{qs} - V_{qgs}}{R} \tag{17}$$

where ω_e, L, R, V_{ds}, V_{qs}, V_{qgs}, respectively, represent the grid angular frequency, line inductances, line resistances, the d-axis inverter voltage, the q-axis inverter voltage, and the q-axis grid voltage. Additionally, by substituting

$$V_{\rm ac} = \sqrt{V_{qs}^2 + V_{ds}^2} \tag{18}$$

in (1), the following equation between the inverter voltages and the inverter gain is found

$$G = \frac{\sqrt{V_{qs}^2 + V_{ds}^2}}{\frac{V_{\rm pv}}{2}}. \tag{19}$$

Moreover, the desired *p.f.* can be associated with the inverter currents by the following equation:

$$\frac{I_{ds}}{I_{qs}} = -\tan\left(p.f.\right). \tag{20}$$

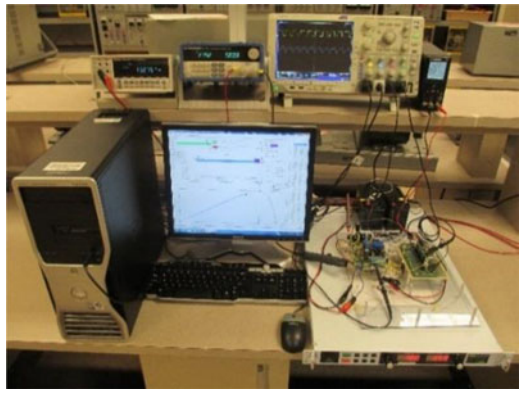

Fig. 6. Experimental setup.

TABLE I
SYSTEM PARAMETERS

Parameter	Value
C_1	1000 μF
C_2	1000 μF
L_1	0.7 mH
L_2	0.7 mH
Sampling time	60 μs
Switching frequency	10 kHz
Cpv	470 μF
Lgrid	1 mH

Knowing the inverter gain and the p.f., (17), (19), and (20) can be solved to find the inverter *q*- and *d*-axis voltages, V_{qs} and V_{ds}. Finally, by knowing V_{qs} and V_{ds}, the phase angle of the inverter voltages can be calculated from

$$\phi_v = \tan^{-1}\left(\frac{-V_{ds}}{V_{qs}}\right). \tag{21}$$

The values of *M* and *D* are generated by the voltage stress minimization block in Fig. 3. Using simple boost control, any inverter gain for a ZSI can be realized using infinite combinations of modulation indices and shoot-through duty ratios. However, inverter gains can be realized using a unique combination of *M* and *D* that will result in the minimum voltage stress on the switches [11], [23], [24]. This combination can be found from

$$M = G \quad D = 0 \tag{22}$$

for inverter gains less than or equal to one, and from

$$M = \tfrac{G}{2G-1} \quad D = 1 - M \tag{23}$$

for the inverter gains more than one.

IV. EXPERIMENTAL RESULTS AND DISCUSSION

The proposed controller is implemented in MATLAB/Simulink and experimentally validated using the dSpace 1103 Hardware-in-the-Loop (HIL) emulator. The experimental setup for this system is shown in Fig. 6. The system parameters are given in Table I. A SUNTECH270S-24-Vb PV module with

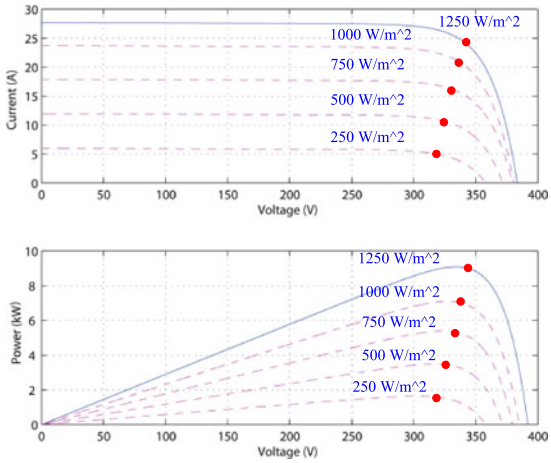

Fig. 7. *P–V* and *I–V* characteristic curves of the employed PV module for experimental verification.

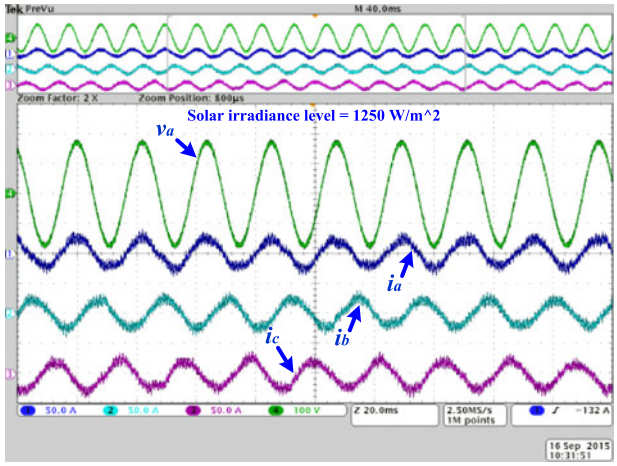

Fig. 9. Three-phase grid-side currents and phase "a" voltage in steady state for solar irradiance level of 1250 W/m^2.

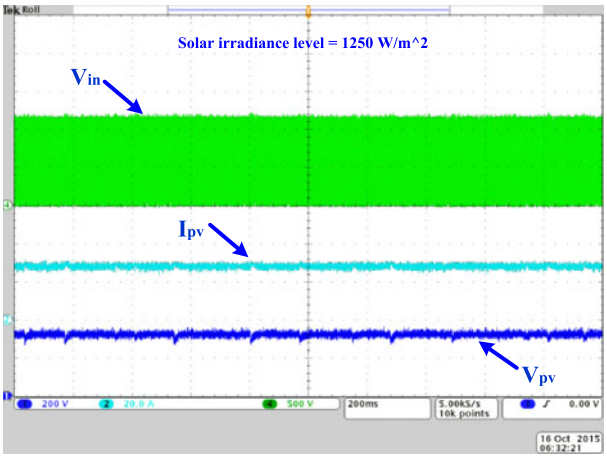

Fig. 8. PV-side voltage and current and the ZSI input voltage in steady state for solar irradiance level of 1250 W/m^2.

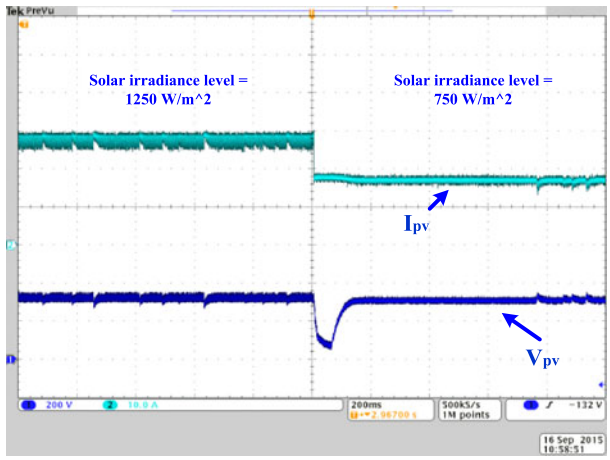

Fig. 10. Response of the PV voltage and current to a step change in solar irradiance.

I–V and *P–V* characteristics shown in Fig. 7 is used as the source of energy for the system. A unity p.f. is targeted for the entire operation. The performance of the proposed model predictive-based MPPT is evaluated by looking into three important merit criteria: the response to a step change in the solar irradiance level, operation in the event of gradually changing solar irradiance (*aka* clouds moving in sky), and operation in steady-state to evaluate the oscillation around MPP.

To begin the analysis, the operation of the system in steady state with solar irradiance of 1250 W/m^2 is explored. The PV-side and grid-side voltages and currents are shown in the scope shots of Figs. 8 and 9. As pictured in Fig. 8, the PV-side waveforms have negligible ripple of less than 2% and the ZSI input voltage is a pulsating high frequency waveform with constant peak at steady state. The grid-side current and voltage waveforms verify the targeted unity p.f. requirement and the calculated total harmonic distortion (THD) of 2.32% from these waveforms is within the IEEE-519 standards for grid-tied systems [41].

In the first experiment, the solar irradiance level is stepped down from 1250 to 750 W/m^2 to analyze the dynamic response of the proposed MPPT system. The expected $I_{\rm pv}$ and $V_{\rm pv}$ from the *I–V* characteristics of the PV modules are, respectively, 24.5 A and 345 V at 1250 W/m^2 and 17 A and 323 V at 750 W/m^2. Fig. 10 illustrates the response of the PV voltage and current to this step change. The results demonstrate fast and accurate dynamic tracking performance with convergence time of less than 10 ms for the proposed model predictive MPPT. The actual measured values of $I_{\rm pv}$ and $V_{\rm pv}$ are 24 A and 342 V at 1250 W/m^2 and 16. 7 A and 319 V at 750 W/m^2, indicating good agreement between the experimental results and the expected outcomes. To analyze the level of voltage and current oscillations around MPP, the waveforms of Fig. 10 are shown in a larger scale (zoomed in) in Fig. 11. According to this figure, the oscillations around MPP are negligible at steady state. The grid-side current and voltage of phase "a" for this experiment are illustrated in Fig. 12. As pictured, the grid-side voltage and current are completely in phase (unity p.f.) with fast dynamic

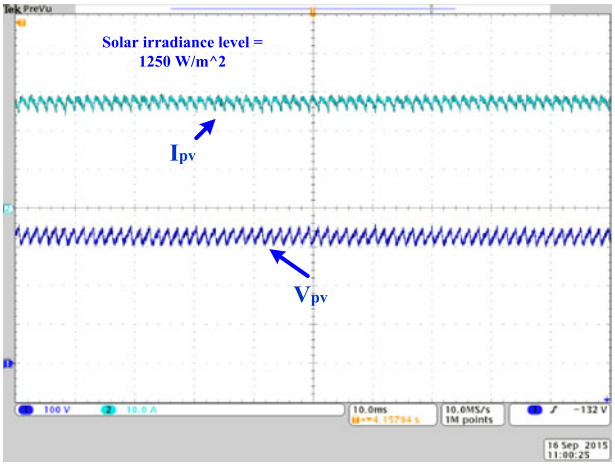

Fig. 11. PV voltage and current ripple at MPP.

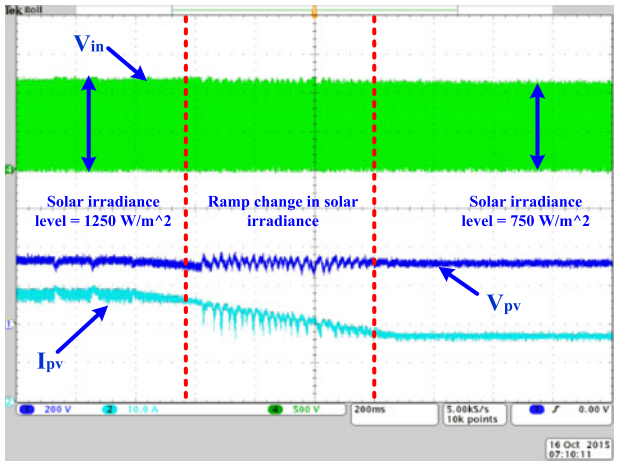

Fig. 13. PV voltage, the ZSI input voltage, and PV current when solar irradiance is gradually decreased from 1250 to 750 W/m^2.

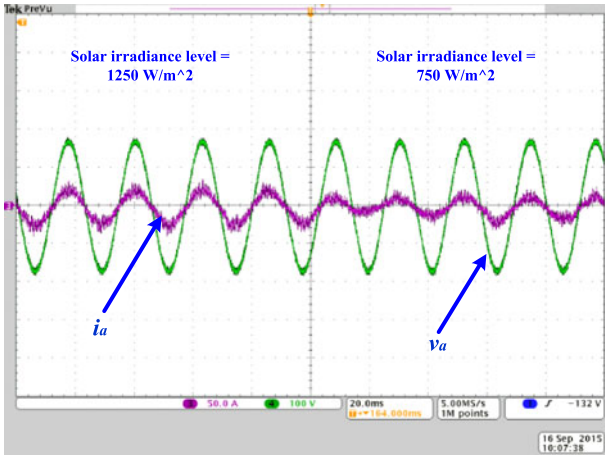

Fig. 12. Grid-side voltage and current of phase "a" in case of a step change in the solar irradiance level.

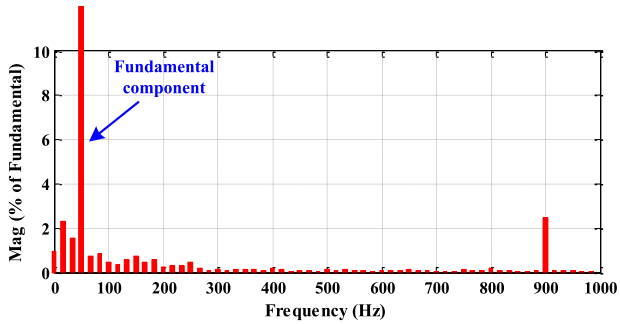

Fig. 14. FFT spectrum analysis of the phase "a" of the grid-side current.

TABLE II
HARMONICS DISTORTION OF GRID-SIDE CURRENT

Harmonics order	Distortion (%)
3rd	0.7%
5th	0.37%
7th	0.18%
9th	0.13%
11th	0.12%
13th	0.05%
15th	0.06%
17th	0.01%

response to the step change in solar irradiance level. The individual harmonic components of the grid current are listed in Table II, and its fast-Fourier transform (FFT) spectrum analysis is illustrated in Fig. 14.

In the second scenario, to evaluate the system performance under more realistic dynamic environmental conditions, a gradually changing solar irradiance test is performed. For this experiment, the solar irradiance was gradually decreased at a rate of 0.85 W/m^2/ms from 1250 to 750 W/m^2 in course of 600 ms. The PV voltage, ZSI input voltage, and PV current waveforms for this experiment are shown in Fig. 13. As pictured, the PV voltage and current are gradually tracking MPP with high accuracy. According to Fig. 13, the ZSI input voltage $V_{\rm in}$ is a high frequency pulsed waveform with a constant peak value when the solar irradiance is constant and a slightly decaying peak value when the solar irradiance gradually decreases.

The control efficacy of the proposed model predictive MPPT is calculated for several solar irradiance levels (from low to high) experimentally and compared to the conventional P&O method (presented in Table III). To calculate the control efficacy, the actual captured power at the PV side for each solar irradiance level is measured and divided by the maximum available power at MPP determined from the *P–V* curves of the utilized PV module shown in Fig. 7. According to Table III, for low to high solar irradiance level, the proposed technique has smaller oscillation ($\Delta P_{\rm PV}$) around MPP and more power capture, thus resulting to MPPT efficacy of more than 99% for all scenarios. Although the P&O exhibits relatively good performance at high solar irradiance levels but the performance degrades significantly for medium to low solar irradiance levels.

The dynamic performance of the proposed model predictive-based MPPT is also compared to the well-known P&O MPPT

TABLE III
EFFICACY COMPARISON FOR THE PROPOSED MPC-BASED MPPT VERSUS P&O METHOD

Solar irradiance level	Conventional P&O method		Proposed model predictive MPPT	
	ΔP_{PV} (%)	Efficacy (%)	ΔP_{PV} (%)	Efficacy (%)
1250	4.21%	98.58%	1.52%	99.03%
1000	4.14%	98.24%	2.47%	99.24%
750	3.94%	98.12%	1.77%	99.07%
500	3.91%	97.43%	2.3%	99.68%
250	3.56%	95.19%	1.65%	99.58%

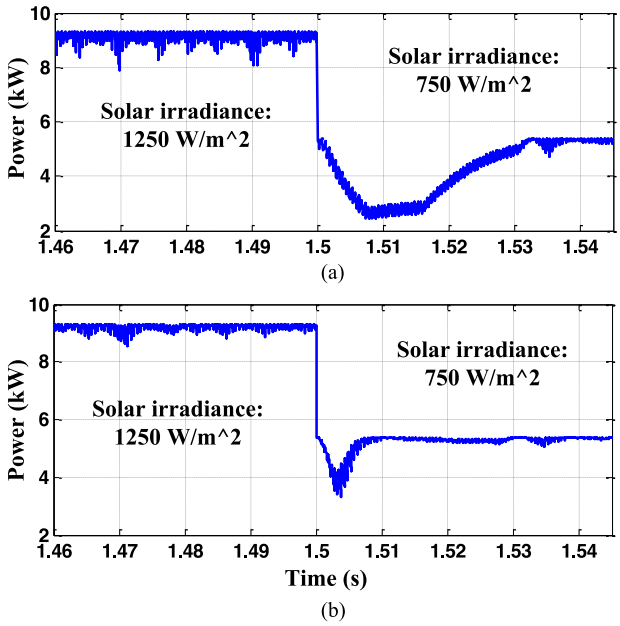

Fig. 15. PV-side response to a 1250 to 750 W/m^2 step change in solar irradiance: (a) conventional P&O technique and (b) proposed model predictive MPPT.

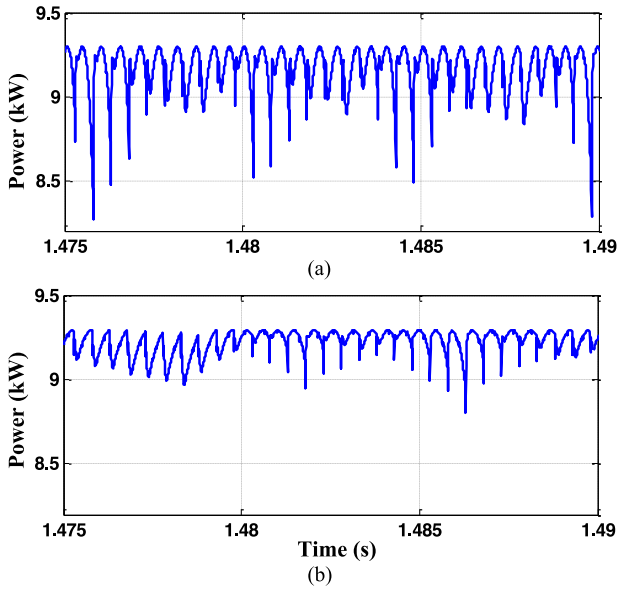

Fig. 16. PV-side power oscillation around the MPP at steady state for solar irradiance level of 1250 W/m^2: (a) conventional P&O technique and (b) proposed model predictive MPPT.

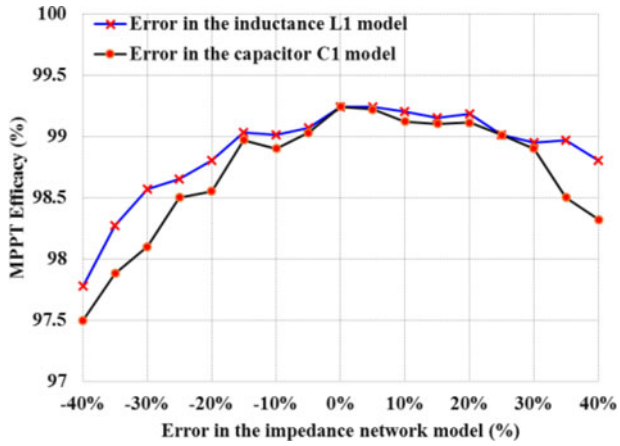

Fig. 17. Effect of the impedance network model error on the MPPT efficacy of the proposed system.

technique for comparative analysis. The results are shown in Figs. 15 and 16. To accurately compare the results side-by-side, the raw data from oscilloscope for the conventional P&O and the proposed method are exported to MATLAB and plotted on the same time axis. As pictured, the proposed technique exhibits better response to a 1250 to 750 W/m^2 step change in solar irradiance level both in terms of convergence time and low oscillations around MPP. According to Figs. 15 and 16, the convergence time of the P&O technique is 35 ms while the convergence time of the proposed technique is only 10 ms. Moreover, the proposed model predictive based MPPT has significantly lower oscillations around MPP comparing to the P&O technique thus eliminating the need of large passive elements in the impedance network.

One of the main drawbacks of the MPC is the effect of model parameters error on the controller performance. In this paper, the robustness and performance of the proposed model predictive MPPT is analyzed for $\pm 40\%$ error in the impedance network model at the PV side of the system; the control efficacy at solar irradiance level of 1000 W/m^2 is calculated and plotted in Fig. 17 for up to $\pm 40\%$ error in L_1 as well as C_1 where 0% error is the nominal inductor and capacitor values (see Table I). In Fig. 17, the error in the models is assumed to be not simultaneously. As it is depicted in Fig. 17, the MPPT efficacy with 0% error is 99.24% and for the worst case scenarios ($+40\%$ or -40% error in the models of C_1 and L_1), the proposed MPPT efficacy is more than 97.5% which still has acceptable performance. It is also interesting to see the MPPT efficacy when multiple errors in the model are happening simultaneously. For this scenario, the errors in C_1 and L_1 are assumed to be happened at the same time; thus, the worst case scenario is when there is $\pm 40\%$ error in the models of C_1 and L_1 at the same time. The MPPT efficacies for this analysis at solar irradiance level of 1000 W/m^2 are depicted in Fig. 18. As it is shown in this figure, even for the worst case scenario the controller has acceptable efficacy of 94%.

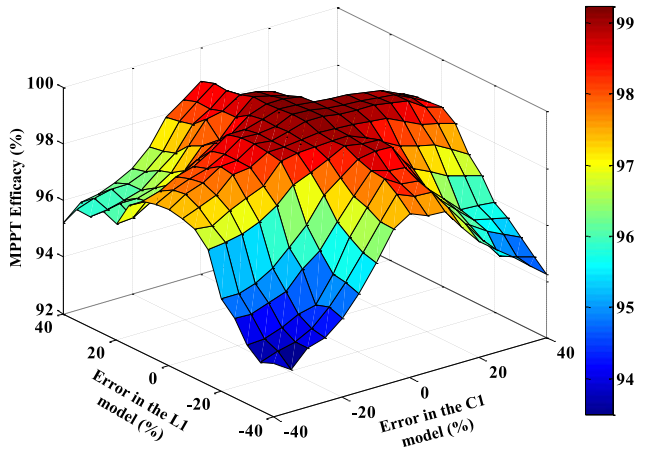

Fig. 18. Effect of the error in the impedance network elements C_1 and L_1 model simultaneously on the MPPT efficacy of the proposed system.

V. Conclusion

This paper presents a highly efficient control scheme for a ZSI-based grid-tied PV system. The presented control system has two components: the proposed model predictive-based MPPT, and the grid-side power injection controller. The experimental results demonstrate low THD of the grid-side current that is within the IEEE 519 standards, fast dynamic response to a step change in solar irradiance level, and negligible oscillations around MPP under dynamically changing sky condition.

References

[1] H. Abu-Rub, M. Malinowski, and K. Al-Haddad, *Power Electronics for Renewable Energy Systems, Transportation and Industrial Applications*. Hoboken, NJ, USA: Wiley, 2014.

[2] S. Kouro, J. I. Leon, D. Vinnikov, and L. G. Franquelo, "Grid-connected photovoltaic systems: An overview of recent research and emerging PV converter technology," *IEEE Ind. Electron. Mag.*, vol. 9, no. 1, pp. 47–61, Mar. 2015.

[3] T. Esram and P. L. Chapman, "Comparison of photovoltaic array maximum power point tracking techniques," *IEEE Trans. Energy Convers.*, vol. 22, no. 2, pp. 439–449, Jun. 2007.

[4] J. Irwin, M. P. Kazmierkowski, R. Krishnan, and F. Blaabjerg, *Control in Power Electronics: Selected Problems*. New York, NY, USA: Academic Press, 2002.

[5] S. Sajadian and E. C. D. Santos, "Three-phase DC-AC converter with five-level four-switch characteristic," in *Proc. Power Energy Conf. Illinois*, 2014, pp. 1–6.

[6] M. Peyvandi, M. Zafarani, and E. Nasr, "Comparison of particle swarm optimization and the genetic algorithm in the improvement of power system stability by an SSSC-based controller," *J. Elect. Eng. Technol.*, vol. 6, pp. 182–191, 2011.

[7] M. I. Chehardeh, H. Lesani, M. K. Zadeh, and E. M. Siavashi, "An optimal control strategy to alleviate sub-synchronous resonance in VSC-HVDC systems," in *Proc. 2nd Int. Conf. Power Electron. Intell. Transp. Syst.*, 2009, pp. 250–255.

[8] N. Farokhnia, M. Ehsani, H. Vadizadeh, H. Toodeji, and M. Mohammad, "Fast closed-form solution of line-to-line voltage total harmonic distortion for three-level inverters," *IET Power Electron.*, vol. 6, pp. 581–591, 2013.

[9] L. Poh Chiang, D. M. Vilathgamuwa, L. Yue Sen, C. Geok Tin, and L. Yunwei, "Pulse-width modulation of Z-source inverters," *IEEE Trans. Power Electron.*, vol. 20, no. 6, pp. 1346–1355, Nov. 2005.

[10] S. Miaosen, A. Joseph, W. Jin, F. Z. Peng, and D. J. Adams, "Comparison of traditional inverters and Z-source inverter for fuel cell vehicles," *IEEE Trans. Power Electron.*, vol. 22, no. 4, pp. 1453–1463, Jul. 2007.

[11] P. Fang Zheng, "Z-source inverter," *IEEE Trans. Ind. Appl.*, vol. 39, no. 2, pp. 504–510, Mar./Apr. 2003.

[12] Y. P. Siwakoti, P. Fang Zheng, F. Blaabjerg, L. Poh Chiang, and G. E. Town, "Impedance-source networks for electric power conversion part I: A topological review," *IEEE Trans. Power Electron.*, vol. 30, no. 2, pp. 699–716, Feb. 2015.

[13] Y. P. Siwakoti, P. Fang Zheng, F. Blaabjerg, L. Poh Chiang, G. E. Town, and Y. Shuitao, "Impedance-source networks for electric power conversion part II: Review of control and modulation techniques," *IEEE Trans. Power Electron.*, vol. 30, no. 4, pp. 1887–1906, Apr. 2015.

[14] M. B. Shadmand, L. Xiao, R. S. Balog, and H. Abu Rub, "Model predictive control of grid-tied photovoltaic systems: Maximum power point tracking and decoupled power control," in *Proc. 1st Workshop Smart Grid Renewable Energy*, 2015, pp. 1–6.

[15] W. Mo, A. P. C. Loh, and B. Frede, "Maximum power point tracking technique implementation of Z-source inverter through finite step model predictive control strategy," in *Proc. 7th IEEE Conf. Ind. Electron. Appl.*, 2012, pp. 1523–1528.

[16] W. Mo, P. C. Loh, and F. Blaabjerg, "Model predictive control for Z-source power converter," in *Proc. IEEE 8th Int. Conf. Power Electron. ECCE Asia*, 2011, pp. 3022–3028.

[17] M. B. Shadmand, R. S. Balog, and H. Abu-Rub, "Model predictive control of PV sources in a smart DC distribution system: Maximum power point tracking and droop control," *IEEE Trans. Energy Convers.*, vol. 29, no. 4, pp. 913–921, Dec. 2014.

[18] G. Baoming, H. Abu-Rub, L. Yushan, and R. S. Balog, "Minimized quasi-Z source network for single-phase inverter," in *Proc. IEEE Appl. Power Electron. Conf. Expo.*, 2015, pp. 806–811.

[19] B. Poorali, A. Torkan, and E. Adib, "High step-up Z-source DC-DC converter with coupled inductors and switched capacitor cell," *IET Power Electron.*, vol. 8, pp. 1394–1402, 2015.

[20] D. Xinping, Q. Zhaoming, X. Yeyuan, and F. Z. Peng, "A novel ZVS Z-source rectifier," in *Proc. IEEE Appl. Power Electron. Conf. Expo.*, 2006, pp. 951–955.

[21] F. Z. Peng, "Z-source inverter for motor drives," in *Proc. IEEE Power Electron. Spec. Conf.*, 2004, vol. 1, pp. 249–254.

[22] T. Yu, Z. Chaohua, and X. Shaojun, "Z-source AC-AC converters solving commutation problem," in *Proc. IEEE Power Electron. Spec. Conf.*, 2007, pp. 2672–2677.

[23] P. Fang Zheng, S. Miaosen, and Q. Zhaoming, "Maximum boost control of the Z-source inverter," *IEEE Trans. Power Electron.*, vol. 20, no. 4, pp. 833–838, Jul. 2005.

[24] S. Miaosen, W. Jin, A. Joseph, P. Fang Zheng, L. M. Tolbert, and D. J. Adams, "Constant boost control of the Z-source inverter to minimize current ripple and voltage stress," *IEEE Trans. Ind. Appl.*, vol. 42, no. 3, pp. 770–778, May/Jun. 2006.

[25] L. Yushan, G. Baoming, H. Abu-Rub, and P. Fang Zheng, "Overview of space vector modulations for three-phase Z-source/quasi-Z-source inverters," *IEEE Trans. Power Electron.*, vol. 29, no. 4, pp. 2098–2108, Apr. 2014.

[26] S. Miaosen, W. Jin, A. Joseph, F. Z. Peng, L. M. Tolbert, and D. J. Adams, "Maximum constant boost control of the Z-source inverter," in *Proc. IEEE Ind. Appl. Conf.*, 2004, pp. 1–147.

[27] D. G. Holmes and T. A. Lipo, *Pulse Width Modulation for Power Converters: Principles and Practice*. Hoboken, NJ, USA: Wiley, 2003, vol. 18.

[28] P. Van den Heever, S. Oberholzer, and J. Enslin, "High-efficient solar panel/wind turbine converter with maximal power control," in *Proc. Eur. Conf. Power Electron. Appl.*, 1989, pp. 663–668.

[29] J. Applebaum, "The quality of load matching in a direct-coupling photovoltaic system," *IEEE Trans. Energy Convers.*, vol. EC-2, no. 4, pp. 534–541, Dec. 1987.

[30] A. Kislovski and R. Redl, "Maximum-power-tracking using positive feedback," in *Proc. IEEE Power Electron. Spec. Conf.*, 1994, pp. 1065–1068.

[31] S. Wolf and J. Enslin, "Economical, PV maximum power point tracking regulator with simplistic controller," in *Proc. IEEE Power Electron. Spec. Conf.*, 1993, pp. 581–587.

[32] H. Dong, H. Sugimoto, and N. Nishio, "A maximum power tracking control method for photovoltaic power generation system based on derivation of output power with respect to output voltage," *Trans.-Inst. Elect. Eng. Japan D*, vol. 118, pp. 1435–1442, 1998.

[33] T. Ouchi, H. Fujikawa, S. Masukawa, and S. Iida, "A control scheme for three-phase current source inverter in interactive photovoltaic system," *Trans.-Inst. Elect. Eng. Japan D*, vol. 120, pp. 230–239, 2000.

[34] A. F. Boehringer, "Self-adapting dc converter for solar spacecraft power supply," *IEEE Trans. Aerosp. Electron. Syst.*, vol. AES-4, no. 1, pp. 102–111, Jan. 1968.

[35] J. Schoeman and J. V. Wyk, "A simplified maximal power controller for terrestrial photovoltaic panel arrays," in *Proc. IEEE Power Electron. Spec. Conf.*, 1982, pp. 361–367.
[36] J. Rodriguez, M. P. Kazmierkowski, J. R. Espinoza, P. Zanchetta, H. Abu-Rub, H. A. Young, and C. A. Rojas, "State of the art of finite control set model predictive control in power electronics," *IEEE Trans. Ind. Informat.*, vol. 9, no. 2, pp. 1003–1016, May 2013.
[37] T. Geyer and D. E. Quevedo, "Multistep finite control set model predictive control for power electronics," *IEEE Trans. Power Electron.*, vol. 29, no. 12, pp. 6836–6846, Dec. 2014.
[38] O. Ellabban, J. Van Mierlo, and P. Lataire, "A DSP-based dual-loop peak DC-link voltage control strategy of the Z-source inverter," *IEEE Trans. Power Electron.*, vol. 27, no. 9, pp. 4088–4097, Sep. 2012.
[39] L. Jingbo, H. Jiangang, and X. Longya, "Dynamic modeling and analysis of Z source converter-derivation of AC small signal model and design-oriented analysis," *IEEE Trans. Power Electron.*, vol. 22, no. 5, pp. 1786–1796, Sep. 2007.
[40] P. C. Krause, O. Wasynczuk, S. D. Sudhoff, and S. Pekarek, *Analysis of Electric Machinery and Drive Systems*. Hoboken, NJ, USA: Wiley, 2013, vol. 75.
[41] *IEEE Recommended Practices and Requirements for Harmonic Control in Electrical Power Systems*, IEEE Std 519–1992, pp. 1–112, 1992.

Sally Sajadian (M'13) received the B.S. and M.S. degrees in electrical engineering from the Purdue School of Engineering, Indianapolis, IN, USA, in 2012 and 2014, respectively. She is currently working toward the Ph.D. degree in electrical and computer engineering at Southern Illinois University, Carbondale, IL, USA.

Her research interests include photovoltaic systems, renewable energy systems, power electronics, and control of power electronics interfaces.

Reza Ahmadi (M'09) received the B.S. degree in electrical engineering from the Iran University of Science and Technology, Tehran, Iran, in 2009, and the Ph.D. degree in electrical engineering from the Missouri University of Science and Technology, Rolla, MO, USA, in 2013.

He is currently an Assistant Professor of electrical and computer engineering at Southern Illinois University, Carbondale, IL, USA. His research interests include modeling, design and control of power electronic converters, electric-drive vehicles, and solar energy systems.